Mater. Res. Soc. Symp. Proc. Vol. 1622 © 2014 Materials Research Society
DOI: 10.1557/opl.2014.73

Supramolecular Self-Assembly Inside Living Mammalian Cells

Yuan Gao,[1,2,3,4] Ryan Nieuwendaal,[2] Boualem Hammouda,[3] Cristina Berciu,[5] Daniela Nicastro,[5] Jack Douglas,[2] Bing Xu,[4] Ferenc Horkay[1]

[1]Section on Tissue Biophysics and Biomimetics, NICHD, NIH; [2]Polymers Division, NIST; [3]NIST Center for Neutron Research; [4]Department of Chemistry, Brandeis University
[5]Department of Biology, Brandeis University;

Introduction

Driven by directional interparticle interactions, *e.g.*, hydrophobic patchy, pi-pi, dipolar, and hydrogen bonding interactions, certain small molecules self-assemble in aqueous solution to form nanofibers (or other nanostructures) and consequently result in hydrogels.[1-5] Because of their inherent advantages such as biocompatibility, biodegradability, and morphological resemblance of extracellular matrix (ECM), supramolecular nanofibers/hydrogels promise applications in cell culture, drug delivery, and tissue engineering.[6-13] Besides the successful incorporation of bioactive molecules in the hydrogelators which perform ECM-like materials outside biological entities,[6,14,15] it is also important to evaluate the distribution of the nanofibers in the intracellular environment and to understand their interactions with cellular components.

Self-assembly of biomacromolecules into fibrillar nanostructures is a fundamental and ubiquitous process in both prokaryotic and eukaryotic cells that is essential for their form and function. While the cytoskeletal filaments (*e.g.*, F-actin, lamin, or microtubules) are essential for cell mechanics,[16] the self-assembly of aberrant proteins into nanofibers is closely associated with neurodegenerative diseases, such as Alzheimer's, Pick's, Parkinson's or Huntington's disease.[17] Due to their importance in cell biology, intracellular protein filaments (normal and abnormal) have attracted research interest on many levels (organismic to molecular). These studies have provided valuable insights, such as the identification of an array of cytoskeleton-regulatory proteins that are responsible for actin-based cellular phenomena,[18] the elucidation of the non-covalent bonds for interconnecting the fibers in intermediate filaments,[19] and the intracellular protein-degradation pathway for removing abnormal protein filaments.[20] This knowledge not only contributes significantly to the understanding of molecular mechanism of intracellular protein filament formation and function, but also lays the foundation for the study of intracellular nanofibers self-assembled or polymerized from exogenous molecules, which is scientifically intriguing and potentially significant, but has barely been explored.[21,22]

Despite the importance of fibrillar self-assembly in cell function and disease, our understanding of the fundamental molecular factors that govern their geometry and stability remain poorly understood. For example, it is not understood why most proteins form amyloid fibers under certain conditions and it is of course important to know what conditions initiate this processes in the case of amyloid diseases so that more rational medical treatments can be designed. In the present work, we investigate a synthetic gelator exhibiting physical characteristics reminiscent of actin, intermediate fibers and other natural protein assemblies and this gelator has the remarkable property of assembling within mammalian cells when introduced to the surrounding medium of the cell. We take this system as a model for fibrillar assembly and study its stability and form both under in

vitro and in vivo conditions by NMR, fluorescence microscopy, transmission electron microscopy (TEM) and correlative light and electron microscopy (CLEM). The present study is a preliminary screening study whose goal is to identify properties and methods suitable for characterizing these complex materials and to determine basic parameters that can be used to control the stability and the existence of these structures.

Enzyme instructed self-assembly motif

Scheme 1. The structure of enzyme instructed self-assembly motif and corresponding fluorophore labeled hydrogelators.

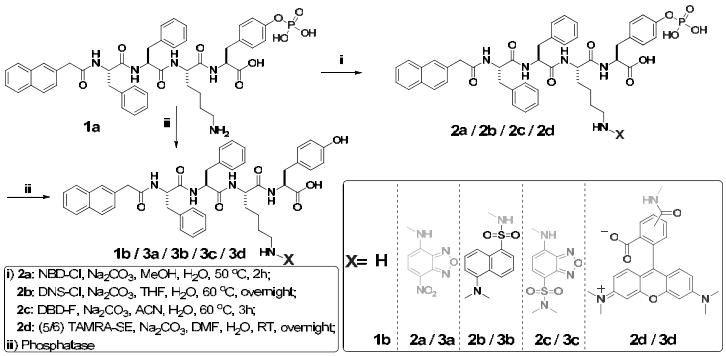

To study supramolecular self-assembly inside living cells, an enzyme instructed strategy is highly desired not only because enzymes are intrinsic components of living cells but also because enzymes are capable to catalyze many chemical reactions in the biological milieu. Scheme 1 shows the structure of a designed molecule (**1a**) which consists of a self-assembly motif and an enzyme (phosphatase) substrate (tyrosine phosphorous ester). While the tetrapeptidic backbone provides the basis for intermolecular hydrogen bonding, the naphthyl group and phenyl groups (on phenylalanine) favor intermolecular aromatic-aromatic interactions. After the enzymatic reaction to remove the phosphorous group, these intermolecular interactions (*e.g.*, hydrogen bonding and hydrophobic interactions) usually facilitate the self-assembly of small molecules in aqueous solutions to form molecular nanofibers.[23] At adequate concentrations, the molecular nanofibers entangle in water and result in a hydrogel.[24] Thus, hydrogelation and/or the formation of nanofibers (or other ordered nanostructures) became a convenient preliminary assay for indicating molecular self-assembly in water.[25]

Transmission electron microscopy (TEM) is a widely applied method to characterize the morphology of the hydrogel (Fig. 1A). Before adding the phosphatase, **1a** molecules hardly self-assemble at low concentration (3 mg/mL) but significantly aggregate as the concentration increases. However, this aggregation is fully thermal reversible (Fig. 1B). For example, around half of **1a** at 9 mg/mL self-assemble at 25 ^{o}C which leads to the observed concentration of 4.7 mg/mL. When the temperature increases to 70 ^{o}C, the observed concentration becomes 9 mg/mL indicating that **1a** is fully dissolved. In contrast, after the addition of phosphatase, none of the hydrogels shows temperature dependence, which implies that enzyme instructed hydrogels are stable in the whole temperature range tested.

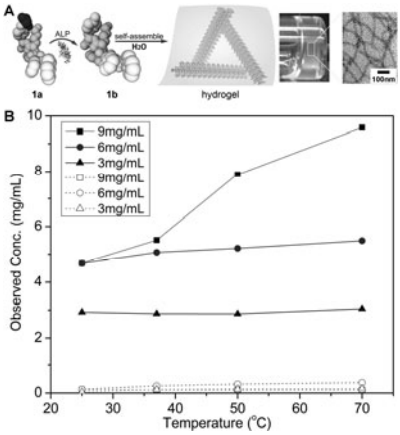

Figure 1. (A) Molecular structure of the precursor **1a**, and the corresponding hydrogelator **1b**. (B) Temperature dependence of the observed concentration of **1a**/**1b** in solution measured by NMR (solid lines: without phosphatase; dot lines: with phosphatase).

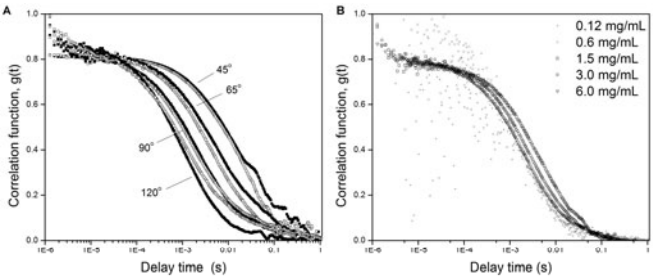

Figure 2. Dynamic light scattering of solutions of **1a** at pH = 7 in water. (A) The angular-dependent scattering intensity indicates the presence of supramolecular aggregates of **1a** (c = 6 mg/mL). The autocorrelation decay curves remain almost the same before (solid) and after (hollow) aging for 48 hours indicating that the aggregates are stable in solution; (B) Scattering decay curves of a serial dilution of **1a** from 6 mg/mL to 0.12 mg/mL. The signal gradually becomes noisy. The critical concentration for the formation of supramolecular aggregates is between 0.6 mg/mL and 0.12 mg/mL.

To determine the critical aggregation concentration (CAC) of **1a**, we used dynamic light scattering (DLS). Figure 2A shows that the DLS autocorrelation functions of **1a** at 6 mg/mL remain unchanged between 2 hr and 48 hr, i.e., the assemblies are stable in solution. The decay curves in Fig. 2B become noisy between 0.6 mg/mL and 0.12 mg/mL, indicating that the critical aggregation concentration (CAC) is between 0.12 and 0.6 mg/mL (141 to 705 μM). After the addition of phosphatase into the solution of **1a**, the dephosphorylated molecule (**1b**, Fig 1A) becomes more hydrophobic that favors self-assembly. For example, at the concentration of 6 mg/mL, there are large amounts of supramolecular assemblies of **1a**, which likely co-assemble with the newly formed molecules **1b** and quickly generate long nanofibers that merely move in solution.

Spatial distribution of fluorophore labeled hydrogelators

We investigated the spatial distribution of each kind of molecules in cellular environment by fluorescent microscopy. We incubated HeLa cells with each precursor (**2a-d**) at the same concentration of 500 μM in PBS buffer. The images show that the fluorescent molecules diffuse into the cells at different rates and at different locations. For example, after adding **2a** to the cells, we found that the fluorescence of **2a** outside the cells remains very weak during the 30 min experiment, which provides a clear background and enables the visualization of the development of fluorescence inside live cells. After 30 min, all the cells glow brighter at the center of cell bodies than around the outer membrane (Fig. 3A).

Unlike **2a**, **2b** is mainly localized in the cell membrane in a relatively homogeneous manner (Fig. 3B). Comparing to **2a**, the low background fluorescence outside the cells confirms that there is insignificant amount of **2b** outside the cells while the different spatial distribution indicates that the assemblies of **2b**/**3b** mainly reside near the cell membrane. Despite the existence of occasional fluorescent dots outside the cells (e.g., the brightest spot in Fig. 3B, middle-right bottom), major portion of fluorophore self-assemble on the cell membrane, which indicates that **2b** likely enter the cells and get dephosphorylated to form **3b** before self-assemble. The distinguishable localizations of the assemblies of **3a** and **3b** reflect different self-assembly propensities due to different fluorophores. The preference of **3b** to the cell membrane likely originates from the dansyl-lysine motif because dansyl-lysine exhibits significantly higher solubility in phospholipid membrane than it does in water[26] and the dansyl group is compatible with the head group of phosphatidylcholine.[27]

2c dissolved in PBS buffer results a highly viscous solution that contains significant amount of nanofibers. Thus, the corresponding confocal image shows that **2c** in PBS buffer forms large amount of fluorescent assemblies only outside the cells (Fig. 3C). During the 30 min incubation, fluorescent assemblies distribute heterogeneously outside the cells and barely change their location, suggesting that the HeLa cells are unable to uptake nanofibers of **2c**.

Although they are unable to form nanofibers and hydrogels, molecules **2d** and **3d** form disordered aggregates. Since the monomers and the aggregates of **2d** and **3d** are highly fluorescent, the whole cell body homogeneously exhibits fluorescence (Fig. 3D) after being incubated with **2d**, though the solution of **2d** outside the cells exhibits significant background fluorescence. Since the molecular structures of **2a** and **2d** only differ in the fluorescent groups and these two fluorescent groups exhibit little specific binding to cellular organelles, the formation of different patterns likely originates from the difference between the self-assembly or aggregation processes.

Thus, the results of fluorescent imaging indicate that **2a**, **2b**, **2c**, and **2d**, though sharing the same self-assembly motif and enzyme responsive residue (i.e., phosphotyrosine), have different propensity of self-assembly, which directly affects the cell response and results in distinct spatial distributions when they interact with live cells.

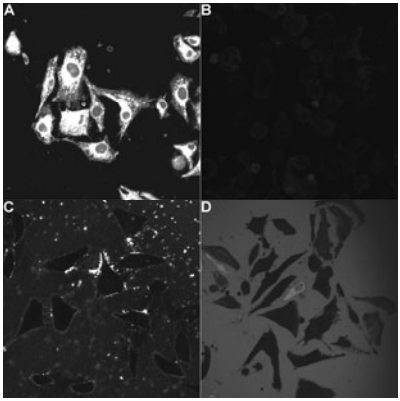

Figure 3. Fluorescent confocal microscope images of the HeLa cells incubated with 500 μM of (A) **2a**, (B) **2b**, (C) **2c**, and (D) **2d** in PBS buffer after 30 min incubation show the different spatial distribution of fluorescent molecules in cellular environment. (each frame: 238 μm x 238 μm).

Intracellular self-assembly originates from the endoplasmic reticulum (ER).

It is important to mention that the spatial profiles of the self- assembly of **3a** are similar. The self-assembly of **3a** mainly occurs at the ER.[28] This presumption is consistent with cell fractionation experiments, which show that the ER containing cell fractions triggers hydrogelation.[29]

We incubated the HeLa cells with **2a** (500 μM) for 1 hour before subjecting the cells to fractionation. The TEM images of the fractions **N**, **M**, and **P** of the treated cell show substantial amount of nanofibers, suggesting that nanofibers form inside the cells (Fig. 4). Although the TEM of fraction **N** shows nanofibers of **3a**, the image in Figure 4 excludes the possibility that nanofibers of **3a** exist in the nucleus. Since the formation of nanofibers of **3a** is protein tyrosine phosphatase (PTP1B)-dependent (*vide infra*) and there is no report of PTP1B in the mitochondria of HeLa cells, it is unlikely that the nanofibers of **3a** form inside the mitochondria. Thus, the observation of the nanofibers in fractions **N** and **M** likely originates from the high molecular weight of the nanofibers of **3a** that makes them more sedimentable. Moreover, the observed nanofibers unlikely are microtubules because no similar nanofibers are present in the control (i.e., HeLa cells without incubating with **2a**). **T**he ribosomal subunit (**R)** and the cytosol (**C**) do not contain nanofibers.

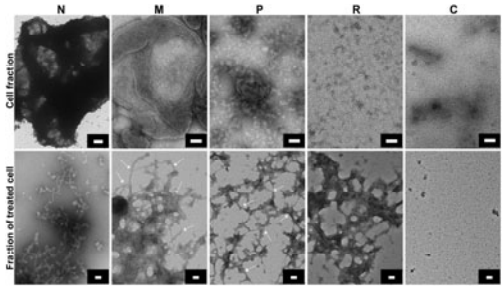

Figure 4. TEM images of the cell fractions before and after enzyme-trigged formation of molecular nanofibers. According to the standard protocol, HeLa cells were fractioned and divided into five parts, named **N**, **M**, **P**, **R**, and **C**. The first row shows the typical morphology from each fraction of HeLa cells. The second row shows the typical morphology from each fraction of HeLa cells, which were pre-incubated with **1a** (500 μM) for 1 hour. Scale bar: 100 nm.

Since PTP1B is a phosphatase known to localize at the cytoplasmic face of the ER,[30] we used an inhibitor PTP1B (CinnGEL 2Me, 25 μM) to co-incubate with the HeLa cells and the precursor (**2a**). We observed delay of the fluorescence (Fig. 5). For example, at 7.5 min, there are no fluorescent cells when the PTP1B inhibitor is present in the medium. After one-hour incubation, most of the cells are fluorescent without the co-incubation of the PTP1B inhibitor, but only a few cells are fluorescent in the presence of the PTP1B inhibitor. This result confirms that PTP1B is the major phosphatase that catalyzes the dephosphorylation of **2a** to result the formation of nanofibers from **3a** in the ER. The rate difference for the *in vivo* experiment and the *in vitro* (i.e., ^{31}P-NMR) experiment may arise from the concentration and activity differences of the phosphatases *in vivo* and *in vitro*. The activity of ALP (Biomatic Co., A1130) has an activity of 3,000 U/mg; the PTP 1B is localized at ER and has an activity of 46,780 U/mg (soluble fractions) and 42,710 U/mg (particulate fractions)[31] (1 Unit = release of 1 nmol phosphate per minute). Since the activity of PTP1B is about 15 times greater than that of ALP, it is reasonable to conclude that the dephosphorylation of **2a** inside the cells occurs one order of magnitude faster than *in vitro*.

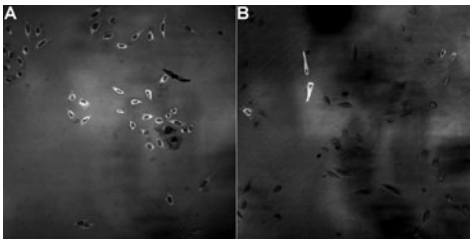

Figure 5. Protein tyrosine phosphatase 1B (PTP1B) dependent self-assembly inside live cells. HeLa cells treated with 500 μM of **2a** without (**A**) or with (B) the PTP1B inhibitor (25 μM) (each frame: 750 μm x 750 μm).

Probing non-fluorescent supramolecular self-assembly in living cells

There are several major limitations of fluorescence labeling such as toxicity or modification of macromolecular interactions.[32-38] To image the self-assembly of small molecules without fluorescence labeling (native form) inside mammalian cells we developed a doping method.[39-41] We found that using dansyl (DNS) labeled molecules makes it possible to localize assemblies formed from non-fluorescent hydrogelator molecules and it allows us to follow the progression of the enzyme assisted self-assembly process.

We used correlative light and electron microscopy (CLEM) to image HeLa cells treated with **1a** and **2b**. This technique allows us to correlate the fluorescence signal of **1b**/**3b**-molecular assemblies imaged in live cells just before their rapid freezing in the EM sample preparation. The ultrastructural organization of the same cells was imaged by TEM (Fig. 6). CLEM reveals a high accumulation of vesicles with low electron-dense material in the cytoplasmic region that shows high fluorescence signal. Moreover, the CLEM experiment on a healthy cell (which adheres and spreads on the grid) establishes the direct correlation between the fluorescent region and the features observed in TEM, which excludes the possibility that the features in TEM arise from cellular stresses that would affect the entire lumen. Although the filamentous assemblies and the bundles are observed in the cytoplasm of the treated (and untreated) HeLa cells, the resolution of plastic section TEM is not sufficient to unambiguously distinguish molecular assemblies from endogenous cytoskeletal intermediate or actin filaments. Molecular assembly-specific electron-dense labels are not available. Therefore, further studies are required for a detailed description of the micro-morphology of intracellular molecular assemblies to verify whether the low electron density material in the vesicles is a hydrogel-forming network consisting of molecular nanofibers.

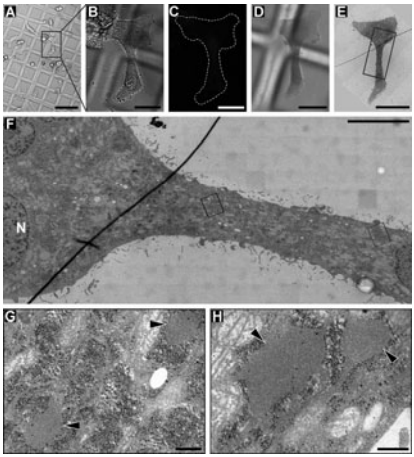

Figure 6. Correlative Light and Electron Microscopy (CLEM) of HeLa cells incubated for 48 h with 500 μM of **1a** and 200 nM of **2b**. (**A-C**) DIC and fluorescence light microscopy images of treated HeLa cells growing on Aclar plastic film; the low magnification DIC overview (A), the zoom-in DIC image (B) of one cell of interest (red box in A) and the zoom-in fluorescence image (B) of the same cell were recorded only a few minutes

before the sample was frozen; note that the Aclar film was marked with a pattern for tracking cells of interest throughout the CLEM sample preparation. In (C) the highest intensity of fluorescence signal in the narrow part of the cell indicates high abundance of hydrogelator in that region of the cell. (**D**) DIC light microscopy image of the same cell shown in (B and C), but after high-pressure freezing, freeze-substitution and resin-embedding; note that the Aclar pattern is still visible to guide trimming of the resin block before cutting ultrathin plastic sections (70 nm thick) that can be inspected in the transmission electron microscope (TEM). (**E**) Low magnification TEM image of the cell of interest shown in (B-D). (**F**) Higher magnification electron micrograph of the neck-region (red box in E) of the same cell shown in (B-E); the narrow neck-region of the cell corresponds to the area of highest fluorescence signal (in C); the image displays a large specimen area at relatively high resolution, because it is a "montage image" that was stitched together from 220 individual, high magnification image tiles. (**G, H**) High magnification electron micrographs of the (G) left boxed area and (H) right boxed area in (F); note the presence of low electron-dense pools (black arrowheads), presumably containing hydrogelator. Scale bars: 100 µm (A), 25 µm (B, C, D, E), and 5 µm (F), 250 nm (G, H).

Conclusions

In conclusion, molecular assemblies formed from small molecules exhibit significantly different behavior from the individual molecules. The reported model system not only allows intracellular formation of nanostructures *via* enzyme-instructed molecular self-assembly, but also offers a new way for elucidating and utilizing the emerging properties of supramolecular assemblies of small molecules inside cells. For example, intracellular formation of molecular assemblies could be used selectively inhibit the growth of cells that overexpress certain enzymes.[21, 22, 42] The further development of molecular self-assembly[43-45] based approaches for understanding and modulating fundamental cellular processes (*e.g.*, proteostasis) and for exploring their potential applications in biomedicine (*e.g.*, intracellular drug delivery[46]), may ultimately lead to a new way to regulate cellular functions. The small size of precursors and the simplicity of the enzyme-instructed self-assembly process should also facilitate the delineation of the molecular details of molecular assemblies from the complex cellular process.

Acknowledgement
This work was supported by the Intramural Research Program of the NICHD/NIH.

Reference

1. L. A. Estroff, A. D. Hamilton, *Chem. Rev.* **104**, 1201 (2004).
2. M. de Loos, B. L. Feringa, J. H. van Esch, *Eur. J. Org. Chem.* 3615 (2005).
3. N. M. Sangeetha, U. Maitra, *Chem. Soc. Rev.* **34**, 821 (2005).
4. R. V. Ulijn, A. M. Smith, *Chem. Soc. Rev.* **37**, 664 (2008).
5. M. Suzuki, K. Hanabusa, *Chem. Soc. Rev.* **38**, 967 (2009).
6. G. A. Silva, *et al. Science* **303**, 1352 (2004).
7. R. J. Mart, R. D. Osborne, M. M. Stevens, R. V. Ulijn, *Soft Matter* **2**, 822 (2006).
8. S. G. Zhang, *Nat. Biotechnol.* **21**, 1171 (2003).
9. H. G. Cui, M. J. Webber, S. I. Stupp, *Biopolymers* **94**, 1 (2010).
10. T. C. Holmes, *et al. Proc. Natl. Acad. Sci. U. S. A.* **97**, 6728 (2000).
11. M. P. Lutolf, *et al. Proc. Natl. Acad. Sci. U. S. A.* **100**, 5413 (2003).
12. C. Q. Yan, D. J. Pochan, *Chem. Soc. Rev.* **39**, 3528 (2010).
13. L. Haines-Butterick, *et al. Proc. Natl. Acad. Sci. U. S. A.* **104**, 7791 (2007).

14. Y. Gao, *et al. J. Am. Chem. Soc.* **131**, 13576 (2009).
15. F. Zhao, M. L. Ma, B. Xu, *Chem. Soc. Rev.* **38**, 883 (2009).
16. D. A. Fletcher, D. Mullins, *Nature*, **463**, 485 (2008).
17. M. G. Spillantini, R. A. Crowther, R. Jakes, M. Hasegawa, M. Goedert, *Proc. Natl. Acad. Sci. U. S. A.* **95**, 6469 (1998).
18. T. D. Pollard, J. A. Cooper, *Science*, **326**, 1208 (2009).
19. M. D. Perng, L. Cairns, P. van den Ijssel, A. Prescott, A. M. Hutcheson, R. A. Quinlan, *J. Cell Sci.* **112**, 2099 (1999).
20. D. C. Rubinsztein, *Nature*, **443**, 780 (2006).
21. Z. Yang, G. Liang, Z. Guo, B. Xu, *Angew. Chem. Int. Ed.* **46**, 8216 (2007).
22. Z. M. Yang, K. M. Xu, Z. F. Guo, Z. H. Guo, B. Xu, *Adv. Mater.* **19**, 3152 (2007).
23. M. L. Ma, Y. Kuang, Y. Gao, Y. Zhang, P. Gao, B. Xu, *J. Am. Chem. Soc.* **132**, 2719 (2010).
24. P. Terech, R. G. Weiss, *Chem. Rev.* **97**, 3133 (1997).
25. Z. Yang, G. Liang, B. Xu, *Acc. Chem. Res.* **41**, 315 (2008).
26. G. M. K. Humphries, J. P. Lovejoy, *Biophys. J.* **42**, 307(1983).
27. E. Abel, G. E. M. Maguire, O. Murillo, I. Suzuki, S. L. De Wall, G. W. Gokel, *J. Am. Chem. Soc.* **121**, 9043 (1999).
28. Y. Gao, J. F. Shi, D. Yuan, B. Xu, *Nat. Commun.* **3**, 1033 (2012).
29. E. Dopp, *et al. Drug Metab. Dispos.* **36**, 971 (2008).
30. J. V. Frangioni, P. H. Beahm, V. Shifrin, C. A. Jost, B. G. Neel, *Cell* **68**, 545 (1992).
31. N. K. Tonks, C. D. Diltz, E. H. Fischer, *J. Biol. Chem.* **263**, 6722 (1988).
32. M. Sameiro, T. Goncalves, *Chem. Rev.* **109**, 190 (2009).
33. M. Zimmer, *Chem. Rev.* **102**, 759 (2002).
34. I. L. Medintz, H. T. Uyeda, E. R. Goldman, H. Mattoussi, *Nat. Mater.* **4**, 435 (2005).
35. U. Resch-Genger, M. Grabolle, S. Cavaliere-Jaricot, R. Nitschke, T. Nann, *Nat. Methods* **5**, 763 (2008).
36. K. Wang, M. E. Rodgers, D. Toptygin, V. A. Munsen, L. Brand, *Biochemistry* **37**, 41 (1998).
37. Y. Taniguchi, P. J. Choi, G. W. Li, H. Y. Chen, M. Babu, J. Hearn, A. Emili, X. S. Xie, *Science* **329**, 533 (2010).
38. C. W. Freudiger, *et al. Science* **322**, 1857 (2008).
39. K. J. Channon, G. L. Devlin, C. E. MacPhee, *J. Am. Chem. Soc.* **131**, 12520 (2009).
40. L. Chen, S. Revel, K. Morris, D. J. Adams, *Chem. Commun.* **46**, 4267 (2010).
41. Y. Gao, C. Berciu, Y. Kuang, J. F. Shi, D. Nicastro, B. Xu, *ACS Nano* (2013) DOI:10.1021/nn403664n
42. G. L. Liang, H. J. Ren, J. H. Rao, *Nat. Chem.* **2**, 54 (2009).
43. I. Huc, J. M. Lehn, *Proc. Natl. Acad. Sci. U. S. A.* **94**, 2106 (1997).
44. J. M. Lehn, *Angew. Chem. Int. Ed.* **29**, 1304 (1990).
45. G. M. Whitesides, J. P. Mathias, C. T. Seto, *Science* **254**, 1312 (1991).
46. Y. Lee, T. Ishii, H. J. Kim, N. Nishiyama, Y. Hayakawa, K. Itaka, K. Kataoka, *Angew. Chem. Int. Ed.* **49**, 2552 (2010).